

**ROLE OF LYMPHATIC ENDOTHELIAL CELL CAVEOLIN-1 IN
MACROMOLECULE TRANSPORT**

An Undergraduate Research Scholars Thesis

by

BRADLEY D. UPCHURCH

Submitted to the Undergraduate Research Scholars program at
Texas A&M University
in partial fulfillment of the requirements for the designation as an

UNDERGRADUATE RESEARCH SCHOLAR

Approved by Research Advisor:

Dr. Joseph M. Rutkowski

May 2017

Majors: Biochemistry
Genetics

TABLE OF CONTENTS

	Page
ABSTRACT.....	1
DEDICATION.....	3
ACKNOWLEDGMENTS	4
NOMENCLATURE	5
CHAPTER	
I. INTRODUCTION	6
Overview of Lymphatic System and Transport.....	6
Lymphatic- Interstitial Interface	7
Caveolae and Caveolin-1	9
II. MATERIALS AND METHODS.....	12
Lymphatic Patterning and Morphology	12
<i>In vivo</i> Dextran Injections.....	12
Primary LEC Isolation	14
Primary LEC Fluorescent Morphology	16
LEC Transwell Transport Permeability Assay	16
Lymphatic Vessel Isolation and Permeability Study	17
III. RESULTS	19
Lymphatic Patterning and Morphology	19
<i>In vivo</i> Dextran Injections.....	20
Primary LEC Fluorescent Morphology	21
LEC Transwell Transport Permeability Assay	23
Lymphatic Vessel Isolation and Permeability Study	25
IV. DISCUSSION.....	27
REFERENCES	33
APPENDIX.....	38

ABSTRACT

Role of Lymphatic Endothelial Cell Caveolin-1 in Macromolecule Transport

Bradley D. Upchurch
Department of Biochemistry and Biophysics
Texas A&M University

Research Advisor: Dr. Joseph M. Rutkowski
Department of Medical Physiology
Texas A&M Health Science Center

The lymphatic system is a network of capillaries, vessels, and nodes that span the length of our entire body. Lymphatic capillaries uptake immune cells, fluid, and macromolecules from the interstitium and transport this lymph through vessels to lymph nodes for immune regulation and tissue fluid balance ultimately returning it to the blood vasculature. How fluid and solutes enter lymphatic capillaries has long been viewed as a passive paracellular mechanism in which macromolecules and fluid enter through valve-like openings in the loosely overlapped cell-cell junctions of lymphatic capillaries. Recent studies have demonstrated that lymphatic endothelial cells (LECs) may utilize pore formation with membrane caveolae as an active transcellular pathway to uptake macromolecules from the interstitium. Caveolin-1 is a protein required for the formation of caveolae and transcellular transport processes. We hypothesized that LECs utilize active caveolae to regulate lymphatic solute transport. To allow us to test our hypothesis, methods for primary LEC isolations and lymphatic vessel isolations had to be developed, established, and successfully tested. To test our hypothesis, we utilized a transgenic mouse carrying loxP sites flanking exon 3 of the Cav-1 gene. When crossed with mice expressing the enzyme Cre recombinase specifically in LECs, we generated mice lacking caveolin-1 in lymphatic

endothelium, and, therefore, LECs incapable of forming caveolae. We utilized this mouse to identify changes in lymphatic uptake and transport of macromolecules over a range of sizes *in vivo*. We isolated and perfused lymphatic vessels from these mice to quantify changes in vessel permeability as a function of solute size. *In vitro*, LECs from these mice, were cultured into monolayers to demonstrate active barrier function to macromolecules. Our data thus identify mechanisms of lymphatic transport that actively regulate solute transport with implications in antigen transport and immune maintenance.

DEDICATION

I would like to dedicate this paper to my parents, peers, and past teachers. These are the people that encouraged my motivation to always work hard to pursue my dreams. I would especially like to dedicate this thesis to two former teachers, Mrs. Denny and Mrs. Pitts, both of which cultivated a love of anatomy and chemistry that laid the foundation for the passion that pushes me every day to strive to achieve my goals.

ACKNOWLEDGEMENTS

I would like to thank Dr. Rutkowski for the countless hours spent teaching me how to think and act like a successful scientist. I would also like to thank my fellow lab members for their help and encouragement.

Thanks also deserves to be given to my friends, family, and colleagues that have played important roles in making my experience at Texas A&M University memorable. Without the support and encouragement from the extraordinary people in my life, I would not be where I am today.

Lastly, I want to specifically thank my parents for instilling the core foundation of my beliefs and motivation into me since I was a child. I would be nowhere without your love and encouragement.

NOMENCLATURE

BEC	Blood Endothelial Cell
Cav-1	Caveolin-1
ECM	Extracellular Matrix
eNOS	Endothelial Nitric-Oxide Synthase
FLOX	Lymphatic Specific Deletion of Caveolin-1
IFP	Interstitial Fluid Pressure
kDa	Kilodaltons
KO	Knock-out
LEC	Lymphatic Endothelial Cell
NO	Nitric oxide
WT	Wild Type
C	Initial Concentration of Dextran
J_s	Flux
J_v	Starling Force
L_p	Permeability
Π	Osmotic Pressure
σ	Osmotic Reflection
P	Hydrostatic Pressure
P_{eff}	Effective Permeability
S	Surface Area
V	Volume

CHAPTER I

INTRODUCTION

Overview of Lymphatic System and Transport

The lymphatic system is vital to our health by directing and controlling the interactions between ourselves and the environment that surrounds us (1). A major role of the lymphatic system is to absorb fluid that regularly extravasates from the blood vasculature (2). This fluid is extravasated due to hydrostatic and osmotic pressure differences and collects in the interstitial space also known as the interstitium (2). If this interstitial fluid is not sufficiently evacuated by lymphatics, it leads to a medical condition called lymphedema (3). Lymphatic vessels, specifically initial lymphatic capillaries, are responsible for removing this fluid and protein from the interstitium to maintain interstitial hydrostatic and osmotic pressure balance (2). Lymph vessels collect this fluid and protein, now called lymph, and return the lymph back into blood circulation for the important purpose of fluid balance and homeostasis (2). In this capacity, the lymphatic vasculature also regulates immune clearance and local immune interactions accomplished by immune cell and antigen trafficking, transport, and delivery to the lymph nodes for interaction. The system's roles in fluid balance and immune regulations are tightly coupled, indeed inseparable, during acute and chronic inflammation (see **Appendix** for an authored review of the subject). While understanding lymphatic transport has clear impacts on immune function, this project focuses specifically on the critical role of lymphatics in macromolecule transport (4).

Lymphatic-Interstitial Interface

While larger lymphatic vessels contain smooth muscle to aid in fluid propulsion, the initial lymphatic capillaries are not surrounded by smooth muscle and are in a partially collapsed state dependent on interstitial fluid pressure and extracellular matrix (ECM) compliance (5). The capillaries are also made up of a continuous layer of lymphatic endothelial cells (LECs) that do not contain any perforations (6, 7), lack basement membranes (8), and tend to line up end to end or slightly overlapping meaning they do not have tight end-to-end junctions (6, 7, 9). To envision these junctions, Baluk and colleagues have described this interface as a series of buttons and zippers (10). This structure tends to favor paracellular permeability for lymphatics to fulfill as the preferred route of macromolecule transport from peripheral tissues.

Paracellular transport is the transport of fluid and molecules between cell-cell contacts that was originally found using an electron microscope looking at rat blood vessel structures (11). In lymphatic vessels, paracellular transport is controlled by anchoring filaments, similar in structure to elastin (12), that attach the basal lamina to the nearby extracellular matrix collagen fibers that expand the luminal volume in response to interstitial stress to take in more fluid into the vessels (5, 13-16). Fundamentally, fluid from the interstitial space can be pushed through the cell to cell junctions, but the overlapping nature of these junctions prohibit retrograde flow of the lymph back into the interstitium (5, 13, 16). Lymph is forced into the vessels by what is called Starling forces that are additive hydrostatic and oncotic forces that cause the movement of fluid across a capillary membrane that can be described by equation 1, below, originally derived to describe blood capillary extravasation.

$$1. Jv = Lp \frac{S}{V} (\Delta P - \sigma \Delta \pi)^1$$

¹ Terms in the equation 1 are defined in the **Nomenclature** section on page 5.

Cells can control permeability to fluid and molecules in constant hydrostatic and oncotic pressure conditions through the use of either paracellular transport or transcytosis. Furthermore, when Starling forces differential is high between the interstitium and the lymphatic lumen, more fluid and macromolecules are forced across the lymphatic barrier and into the cell by paracellular transport. It is a misconception to think of open lymphatic capillaries as having luminal hydrostatic and osmotic pressures equal to the interstitium. Downstream lymphatic vessel pumping provides a subtle pressure gradient for entry, and the vessel wall, and any openings therein, provide a reflection coefficient for solute size-dependent uptake.

The second mechanism of transport across an endothelial barrier is transcellular transport or transcytosis. Transcytosis is the movement of fluid and molecules across membranes using the process of endocytosis (6, 7, 17). Using more extensively studied blood endothelium as a model of barrier function, studies have shown that blood capillaries utilize transcellular pathways to uptake macromolecules from the interstitium into the blood vasculature lumen (18). Macromolecules, including albumin, are unable to be transported through the small overlapping cell-cell junctions because they exceed a 3 nm globular structure and are instead specifically bound and transcytotically transported or generically taken up through non-specific endocytosis. These processes utilize caveolae which are localized in the cell membrane and consist of high levels of a protein called caveolin-1 (among others) (18, 19). Studies have also shown that when there is an increase in pressure in the interstitium, transcytosis increases to combat the increase in transmural pressure (20, 21). Increased blood pressure, or a lack of pore formation in blood endothelium likewise increase extravasation. (22, 23). The relative ease of paracellular flux into lymphatic capillaries has previously discounted transcellular mechanisms in LECs (24). However, the continuous layer of LECs that make up lymphatic capillaries are full of 50-100 nm caveolar

invaginations that function in transporting large and small soluble macromolecules across the membrane into lymphatic capillaries which is defined as transcytosis or endocytosis (25-28); recent studies have shown that the lymphatic endothelium is not simply a passive barrier but has active transport capabilities for macromolecule transport (29-31). Most recently, a study was conducted that specifically tested the importance of intracellular transport (transcytosis) in lymphatic endothelial cells and successfully showed that transcytosis is an important pathway for lipid and solute transport in lymphatic endothelial cells (24). While this data is enlightening, we are interested in determining what protein is important for lymphatic transcytosis. To answer this, we will be focusing on Caveolin-1 found in caveolae.

Caveolae and Caveolin-1

Caveolae have been characterized as crucial structures for transcytosis (27). Caveolar membranes are omega-shaped lipid rafts composed of cholesterol and sphingolipids and multiple structural proteins with some, the family of Caveolins (including Caveolin-1, Caveolin-2, and Caveolin-3), being specific to caveolar structures. While the makeup of caveolae vary from cell to cell, genetic studies have identified that the 21-24 kDa scaffolding protein Caveolin-1 is the single protein absolutely requisite for caveolae formation (32-37). As the essential protein for caveolar function, this project seeks to understand the importance of Cav-1 in transcytosis and lymphatic fluid transport.

Most of the experiments in the paper will be dealing with wild type (WT) mice versus Caveolin-1 KO mice specifically in lymphatics (Cav-1^{flox/flox}) and globally (KO). These mice were created using a Cre-floxP system called Cre-Lox recombination. In this system, in floxP sites flank the gene of interest and with the addition of the Cre recombinase enzyme, the Cre-recombinase

proceeds bind to the loxP site and loop out the gene of interest creating a KO. An animation of the construction of these strains can be seen in Figure 1. Cav-1 protein is then absent from lymphatic endothelium of Floxed mice (Figure 2).

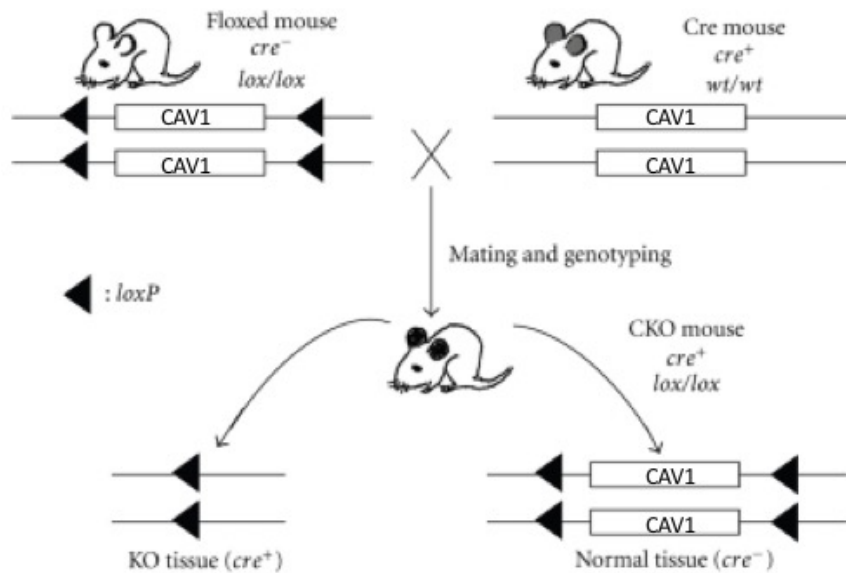


Figure 1. Creation of CAV-1 KO Mouse. Here we used Cre-Lox recombination to create CAV-1 KO mice. Essentially, the Cre, when added, attaches to the loxP site flanking the gene of interest and forces the DNA to loop out the gene of interest leaving the mouse a KO.

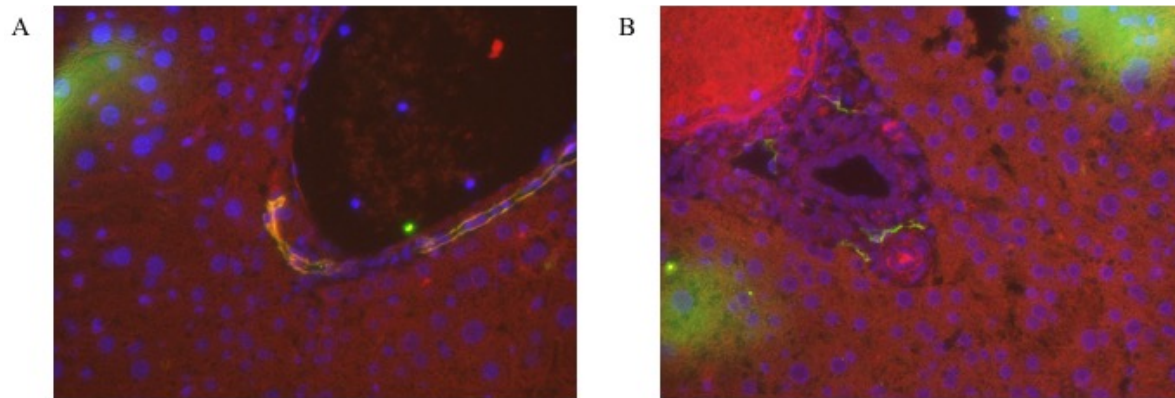


Figure 2. Caveolin-1 Levels in WT and FLOX lymphatic endothelial cells. Liver sections were visualized for lymphatic vessels as hepatocytes express little Caveolin-1. A) Caveolin-1 (red) co-localizes with lymphatic endothelial cells (LYVE-1; green) making an orange/yellow color. B) Only the green LYVE-1 label is seen in in FLOX LECs because there is no Cav-1 present in lymphatics.

Notable Cav-1 KO phenotypes are 1) organisms are still viable and while they show trouble executing endocytosis, the LECs show hyperproliferation (indicating tumor suppressor activity) and loss of caveolin-2 expression (38, 39) and 2) KO mice exhibit hyperpermeability (40). The fact that Cav-1 KO mice show hyperpermeability is interesting because the mice lack caveolae, which should mean that they lack the ability to execute transcytosis which should mean a decrease in permeability. But, hyperpermeability is observed meaning an increase in paracellular transport must be counteracting the loss of transcellular transport (40).

This study focuses on successfully developing methods for isolating primary lymphatic endothelial cells and isolation of intact lymphatic vessels for permeability studies to more accurately study the role of lymphatic caveolar transport in lymphatic macromolecular transport functions.

CHAPTER II

MATERIALS AND METHODS

Lymphatic Patterning and Morphology

Ears were taken from mice with the genotypes wild type (WT), lymphatic specific Cav-1 knock out (FLOX), and global Cav-1 knock out (KO). These ears were then carefully dissected, separating the front and rear halves, and placed in a well in a 96 well flat bottomed plate. After splitting, the ears were incubated in 150 μ L of anti-mouse LYVE1 antibody (1:200 dilution; R&D Systems) for 24 hours in a plate rocker in the 4 °C refrigerator. The ears were then taken out of the anti-mouse LYVE1 and washed two times in 150 μ L of PBS before being transferred to 150 μ L of the Donkey anti-goat (1:400 dilution; Life Technologies) secondary antibody for 24 hours in the 4 °C refrigerator. After the 24-hour incubation, the ears were then washed twice in 150 μ L of PBS before being mounted on microscope slides. The slides were then imaged under a fluorescent microscope and analyzed for vessel width, length, and number of branch points using ImageJ software.

***In Vivo* Dextran Injections**

Using two 3/10 cc syringes, a mouse was injected in both of its hind footpads with 20 μ L of two mixtures of fluorescent dextrans. Mixture 1 was composed of a 3 kDa Fluorescein dextran and a 70 kDa Texas Red dextran that were each at 2 mg/mL final concentration. Mixture 2 contained a 70 kDa Texas Red dextran and a 2,000 kDa Fluorescein dextran that were each at 2 mg/mL final concentration. Figure 3 shows the injection site and lymphatic travel.

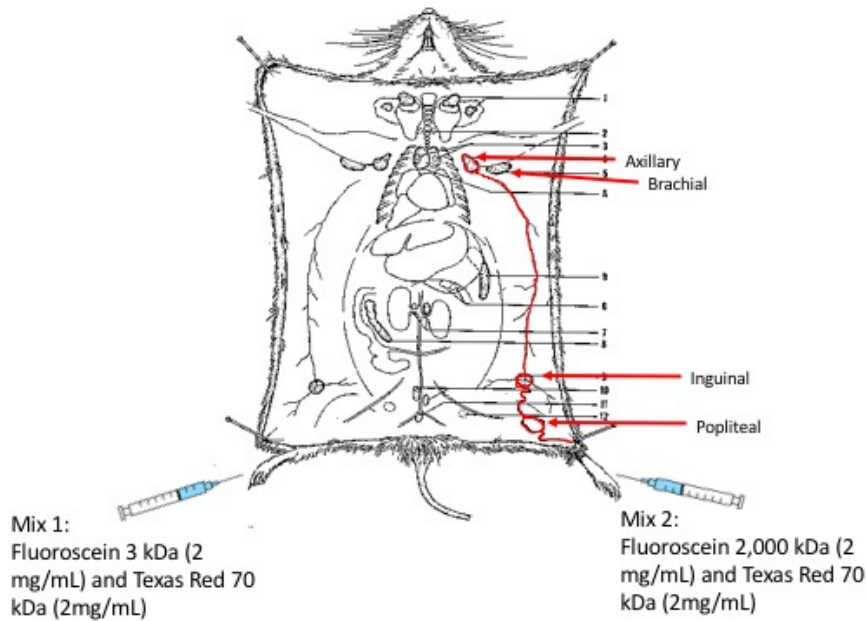


Figure 3. Footpad Injection Method. This figure shows the injection site and procedure along with the dextran pathway of travel through the lymphatic system.

All dextrans were molecular probes from Life Technologies. Injections on the mice were done under isoflurane anesthesia. Forty-five minutes after injection, the mice were sacrificed and the tissues taken included: a skin sample from the footpad, inguinal LN, popliteal LN, and axillary LN. These tissues were then homogenized in a Fisher Scientific Bead Mill 24 for 1 minute in 1 mL tubes with 100 μ L of Radioimmunoprecipitation assay (RIPA) buffer and 0.1 mm zirconia/silica tissue disruption beads. After homogenization, the samples were centrifuged at 21.1 xg for 10 minutes. Next, 50 μ L of each sample were pipetted into a well on a 96 well plate to assess fluorescence levels. After fluorescence levels were determined, 2 μ L of the samples and 23 μ L of RIPA buffer were added to 200 μ L of BCA reagents from a Thermo Scientific Pierce BCA Protein Assay Kit and incubated for 15-30 minutes and analyzed for protein concentration. The results are expressed as a ratio of sample fluorescence to protein concentration.

Primary LEC Isolation

Five mice were sacrificed to obtain the popliteal, inguinal, axillary, and brachial lymph nodes as well as the intestinal mesentery and diaphragm. These tissues were then minced for 10 minutes in an autoclaved 10 mL beaker. The minced tissue was then digested for one hour in a 37°C shaking water bath in an enzyme digestion solution containing 10 mL of digestion buffer, 50 mg Sigma-Aldrich Collagenase D, 100 mg Fisher BioReagents Bovine Serum Albumin (Fraction V), 10 mg Sigma Dispase II, and 1 mg of Roche Liberase DH Research Grade. The digestion buffer consists of HEPES buffer (100 μ M), NaCl (120 mM), KCl (50 mM), Glucose (5 mM), CaCl₂ (1 mM), and water. After digestion was complete, the cells were centrifuged for 5 minutes at 500 xg. The layer of fat that accumulated at the top was then aspirated off. The cells were then resuspended in the digestion solution and filtered through a 100 μ m filter top with an addition of 10 mL of basal DMEM. The cells were then centrifuged for 10 min at 300 xg, and the media was aspirated off. Centrifugation and aspiration were then repeated. After aspiration, the pellet of cells was resuspended into 1 mL of basal DMEM in a 1.5 mL Eppendorf tube. Next, 10 μ L of Biotin Rat Anti-Mouse CD31 (0.5 mg/mL) antibody were added to the cells. The cells were then incubated on a circular rotator for 60 min. After incubation, the cells were centrifuged at 6.1 xg for 5 min, and the media was aspirated off to remove unbound antibody while the cells were resuspended in 1 mL of basal DMEM. This centrifugation and aspiration was repeated two more times. The cells were then resuspended in 1 mL of basal DMEM and 10 μ L of Invitrogen Dynabeads M-280 Streptavidin (10 mg/mL) magnetic beads were added to the cells. Again, the cells were incubated on a circular rotator, but this time for 40 min. After incubation, the cells were placed in a magnetic chamber for 2 minutes with minor movement while the magnetic beads collected near the side of the Eppendorf tube. The extra basal media was pipetted off, and the cells

were resuspended in 1 mL of basal media. This step is repeated two more times. But, on the last aspiration, the cells are resuspended in 1 mL of 10% Fetal Bovine Serum (FBS) full media supplemented with VEGF-C (50 ng/mL). The resuspended cells were then added to a collagen coated 60 mm plate along with 3 mL of 10% FBS +VEGF-C and incubated at 37°C with 5% CO₂ for 24 hours. After 24 hours, the media was changed. Media changes continued every 48 hours for 1 week or until 80-100% confluency.

Once the cells reached 80-100% confluency, flow sorting was used to separate out true LECs from fibroblasts. In this step, cells were trypsinized with 1 mL of trypsin and centrifuged at 600 xg for 5 minutes. The cells were then resuspended into 1 mL of FACS buffer (PBS+0.5% FBS). After resuspension, 30 µL of cells were added into three Eppendorf tubes labeled negative control, LYVE-1 positive, CD-31 positive, and the remaining cells became the sample tube. After distribution, the cells were centrifuged at 6.2 xg for 1 minute and aspirated and resuspended in their corresponding antibody solution. The negative tube had cells resuspended in 100 µL of FACS buffer, while the LYVE-1 and CD-31 tubes contained 100 µL of anti-mouse LYVE-1 (1:200) and anti-mouse CD-31 (1:400). The sample tube cells were resuspended in 100 µL of an antibody solution containing both anti-mouse LYVE-1 and anti-mouse CD-31. The LYVE-1 antibody used a Thermo Fisher Alexa Fluor 488 nm dye, while the CD-31 antibody used a Thermo Fisher Allophycocyanin (APC) 600 nm dye. After 10 minutes of incubation, the cells were spun down again and resuspended in FACS buffer and filtered. After filtering, the cells were centrifuged and resuspended in full media and sorted using a BD FACSAria II system. Cells that were positive for both CD31 and LYVE-1 were isolated and utilized as LECs. The sorted cells were then seeded into 6.5 mm transwell inserts at a concentration of 60,000 cells/ cm².

Primary LEC Fluorescent Morphology

LECs were isolated and cultured following the methods from Primary LEC Isolation. After 12 days of culturing in 20% FBS, the cells were fixed by adding 1 mL of chilled 100% methanol to the cells on ice for 2 minutes. The methanol was then aspirated off and 900 μ L of PBS and 100 μ L of FBS were added to the plate along with an anti-mouse LYVE-1 antibody (R&D Systems) at a 1:200 dilution factor. The cells were then incubated overnight in the 4°C refrigerator. LYVE-1 was visualized with a Donkey anti-goat secondary antibody (1:400; Life Technologies). DAPI (4',6-diamidino-2-phenylindole- a fluorescent stain) was then added to the cells to help visualize each individual cell nuclei. A fluorescent microscope was then used to visualize the cells.

LEC Transwell Transport Permeability Assay

We closely followed the protocol for the Endothelial Permeability Assay used by the Swartz and Rutkowski labs (24, 29, 41). The LECs from WT and FLOX mice that were sorted using flow cytometry were then seeded into a 3 μ m pore sized 6.5 mm Corning Transwell insert. The cells were then grown in 20% FBS+VEGF-C until a full confluent monolayer was observed (96-120 hours). Once confluent, a dextran solution containing a Texas Red 3 kDa (1 mg/mL) and a Fluorescein 2,000 kDa (2 mg/mL) was added to the transwell insert at a concentration of 10 μ g/mL. After 4 hours, 70 μ L was taken from the top of the insert and the media below and run for fluorescence. Permeability was calculated as effective permeability (Equation 2) and relative effective permeability (Equation 3).

$$2. P_{eff} = \frac{J_s}{\Delta C * S}$$

$$3. P_{relative} = \frac{P_{eff(2,000\text{ kDa})}}{P_{eff(3\text{ kDa})}}$$

These transwell experiments are meant to model initial lymphatic capillaries uptake of fluid and macromolecules from the interstitium at the lymphatic-interstitial interface.

Lymphatic Vessel Isolation and Permeability Study

One mouse was sacrificed and dissected so that the skin section with the inguinal and axillary LNs were openly viewed. This set up can be seen in Figure 4. The tissue was covered with Krebs-Henseleit (KH) buffer +1% Bovine Serum Albumin (BSA) to balance the osmolarity. Then, using a Zeiss AxioCam MRc microscope, lymphatic vessels were found by finding a bundle of an artery and a vein that then has two lymphatic vessels on either side. The lymphatic vessel was dissected free from the fat and the artery/vein bundle. After the lymphatic vessel was dissected free and cleansed of remaining excess fat, it was sutured on the upstream end closest to the axillary LN using ophthalmic sutures. The vessel was then cut out and transferred to the cannulation chamber.

The chamber contained 1 mL of the KH+1% BSA buffer solution and a cannulation pipet with a bore size of 60 μm . The vessel was then taken and attached to the cannulation pipet. Once attached, the vessel was sutured to the pipet to ensure that it would not slip of the end when pressurized. Next, the original suture on the free end was cut off and sutured again. Lastly, the vessel was pressurized at 3 cm with two different dextran solutions. Mix 1 contained a 3 kDa Texas Red dextran (1 mg/mL) and a 2,000 kDa Fluorescein dextran (2 mg/mL), while Mix 2 consisted of a 70 kDa Texas Red dextran (2 mg/mL) and a 2,000 kDa Fluorescein dextran (2 mg/mL). Lastly, 10 μL of the chamber solution was taken every 10 minutes for an hour and analyzed using fluorescence. This entire vessel isolation set up can be seen in Figure 4. Vessel Isolation experiments were conducted to model the transport of fluid and macromolecules in larger

lymphatic vessels in between lymph nodes. In future experiments, this isolated vessel experiment could be used to measure vascular tone.

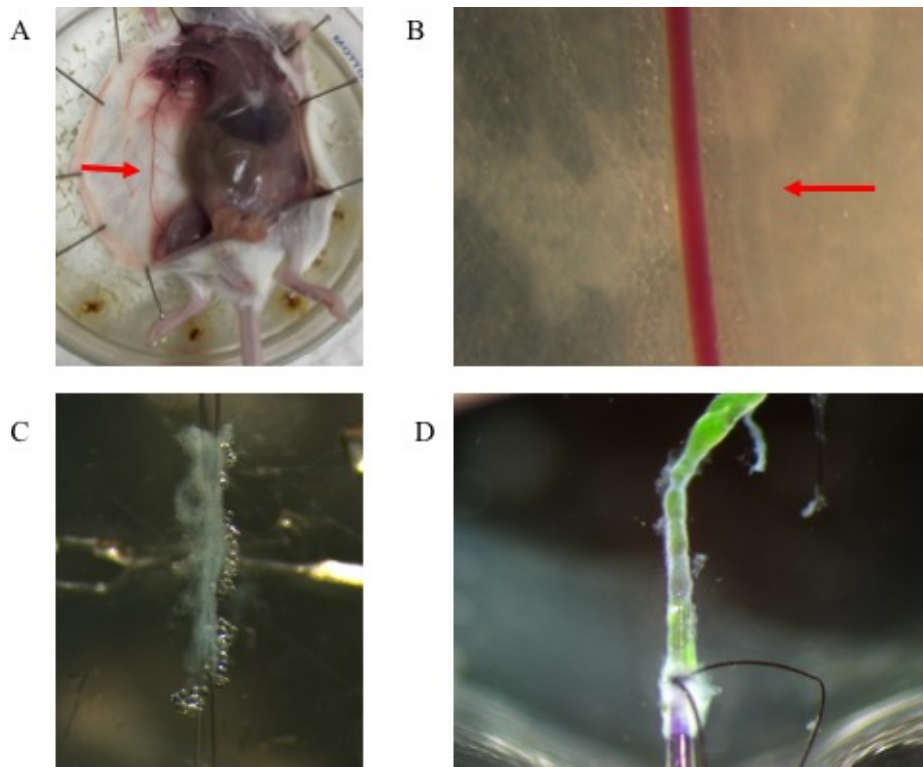


Figure 4. Lymphatic Vessel Isolation and Cannulation. A) One mouse was sacrificed and pinned so that the inguinal-axillary lymphatic pathway was visible. The pathway is labeled with a red arrow. B) The red structure is an artery while the very faint but clear colored tube is the lymphatic vessel of interest and is labeled with a red arrow. C) Two cannulation pipets (60 μm radius) are connected by the lymphatic structure. D) A full vessel is isolated, sutured, cannulated, and pressurized with a fluorescent dextran mixture.

CHAPTER III

RESULTS

Lymphatic Patterning and Morphology

Wild type (WT) and Cav-1^{flox/flox} (FLOX) ears showed normal lymphatic architecture and patterning, while Cav-1 global knock out (KO) mice showed slightly hyperplastic lymphatic vessels (Figure 5). After quantification, WT and FLOX lymphatics had similar branches per vessel length and average vessel widths, while KO lymphatics showed a tendency to increase in both branches per vessel length and average vessel width [n=2; p=0.119] (Figure 6). Overall, there are no statistically significant differences in lymphatic patterning and morphology in FLOX mice.

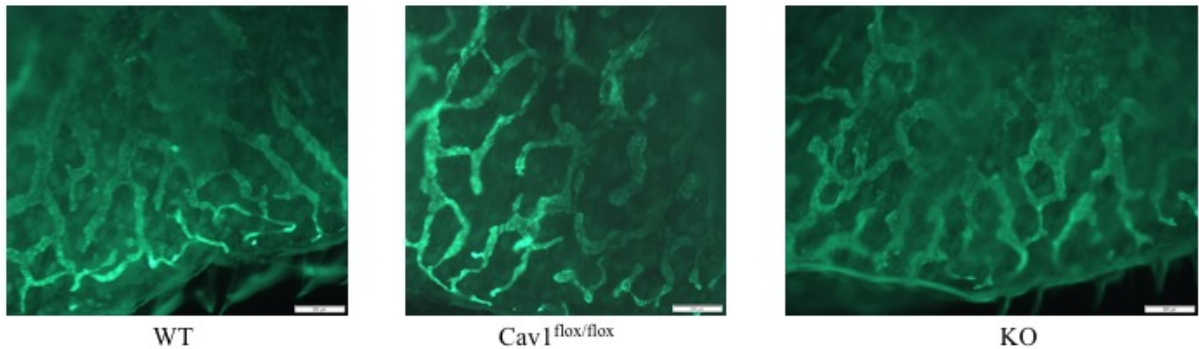


Figure 5. Lymphatic Patterning and Morphology. Mouse ears were fluorescently stained and imaged using anti-LYVE1 (1^o) and donkey anti-goat (2^o)

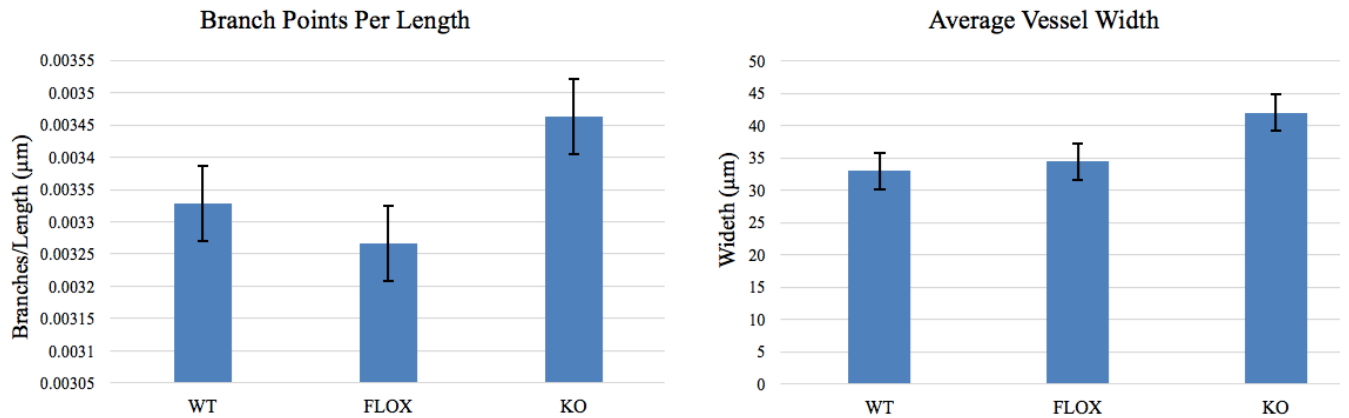


Figure 6. Quantification of Lymphatic Patterning and Morphology. ImageJ software was used to analyze each genotype (n=2). No statistically significant changes were observed.

***In vivo* Dextran Injections**

After injection of the tissues with the different dextran mixtures, the data was collected using a ratio of fluorescence to protein concentration. After analysis, it was observed that there are no statistically significant changes in transport based on genotype or dextran size. All dextrans seemed to be taken up and transported with similar efficiencies creating a decaying trend beginning with the skin and ending with the axillary node (Figure 7). However, although there is no difference observed in the overall uptake and transport, the two lymphatic functions are present *in vivo*. In the first, lymphatic capillaries are taking up the injected dextran from the skin. In the second, this dextran in the lymph must be transported far downstream through the series of lymph nodes. We thus utilized two separate lymphatic models *ex vivo* to mimic initial uptake by capillaries and transport by larger vessels using transwell experiments and vessel isolations, respectively.

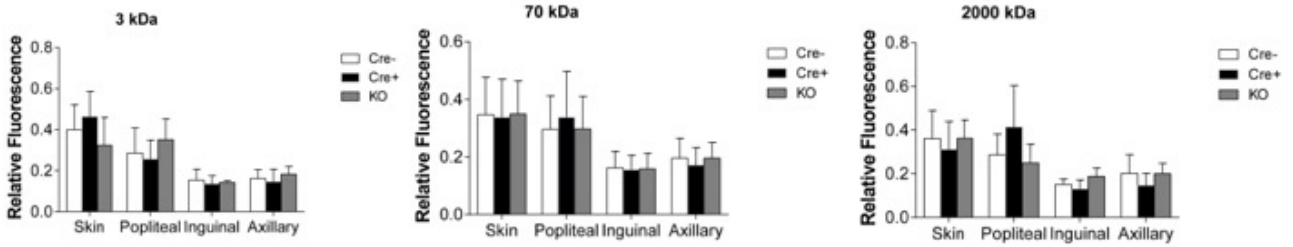


Figure 7. Injection Results. Three different dextrans were used and each dextran was tested in three different mouse genotypes: WT, FLOX (CAV-1 locally deleted in lymphatics), and KO (CAV-1 globally deleted).

Primary LEC Isolation and Morphology

After staining with the LYVE-1 antibody and DAPI, the cells imaged were seen to form into tube structures (Figure 8).

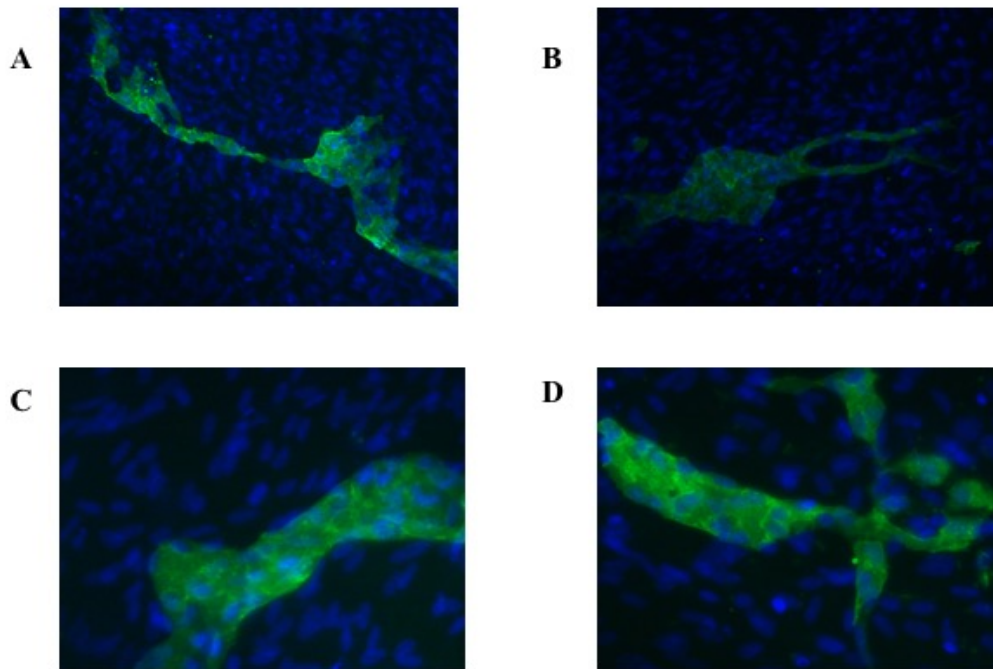


Figure 8. Lymphatic Tube Morphology: Green fluorescence is the LYVE-1 stain that illuminated LECs, while the blue fluorescence is the DAPI stain that illuminated nuclei. A) Imaged at 10X. Showing multiple tube structures connecting to each other to make a single tube. B) Imaged at 20X. Showing two tails of tubes splitting off. C&D) Imaged at 40X.

The LECs grew as if they were *in vivo* showing the native tubular structure that is rarely seen on cultured plates (Figure 8). The green fluorescence is the LYVE-1 antibody that stains LECs, while the blue fluorescence is the DAPI stain that binds to DNA to visualize cellular nuclei. Therefore, the background blue dots of fluorescence are nuclei of other cells that are growing on the plate that have not been tagged by the LYVE-1 antibody because they are not LECs, but most likely fibroblasts. But, in the LEC tube structures we can clearly see at 40X magnification that the tube is made up of many LECs that have grown together in tubes rather than spreading out in a planar fashion demonstrating a “cobble stone” growth pattern. This shows that when LECs are cultured on top of a bed of contaminating fibroblasts, they revert to growing as if *in vivo* to reach out and connect with other LEC cells.

However, the cell population from Figure 8 were not a pure LEC population. To obtain a pure LEC population, the LEC isolation protocol from the Material and Methods Section was conducted and cells were subsequently flow sorted after one week of culture.

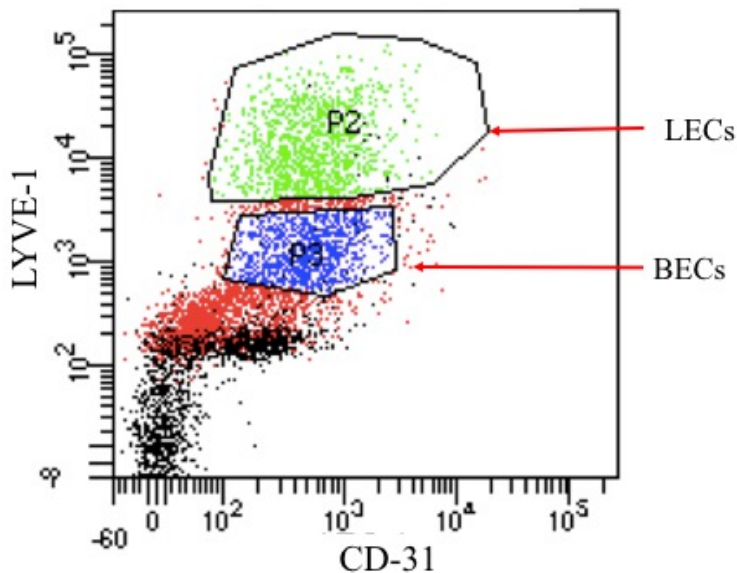


Figure 9. LEC Flow Sorting Results. A pure population of LECs are indicated above being both LYVE-1 and CD-31 positive.

LYVE-1 levels indicate the presence of lymphatic specific cells, while CD-31 levels indicate endothelial cells. So, our population of lymphatic endothelial cells should be both highly positive in both LYVE-1 and CD-31, while contaminating blood endothelial cells (BECs) will be CD-31 positive but not LYVE-1 positive (Figure 9). These results clearly indicate that we were successfully able to isolate a pure culture of LECs (Figure 9). However, initial isolated LECs were merely wildtypes for a proof-of-concept study. So, another isolation and sort was conducted to obtain pure LECs from WT, FLOX, and KO genotypes. Pure LEC populations were obtained from all three genotypes (Figure 10). We were able to sort 61,000 LECs from WT culture, 80,000 LECs from FLOX culture, and 150,000 LECs from KO culture.

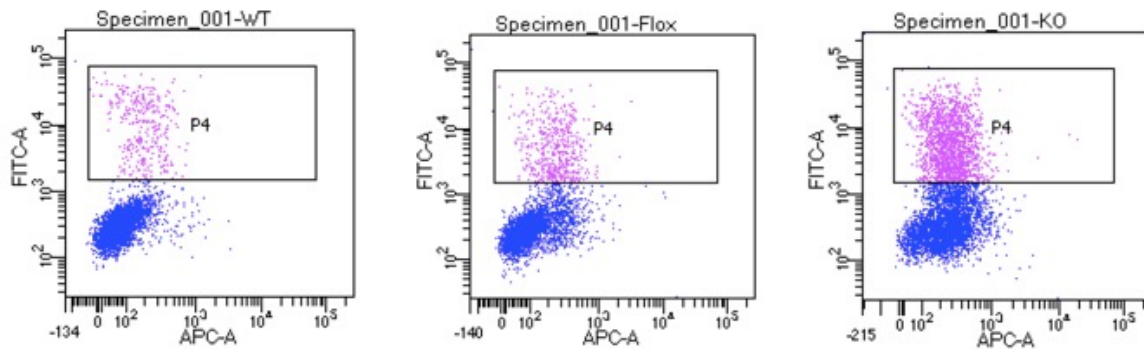


Figure 10. Flow Sort Results from WT, FLOX, and KO cell types. Pure populations of LECs were sorted for all three genotypes by finding cells that were both LYVE-1 and CD-31 positive. The purple area represents LECs, while the blue area represents contaminating BECs. The KO genotype had the most LECs with 150,00 while WT and FLOX had 60,000 and 80,000 cells respectively.

LEC Transwell Transport Permeability Assay

The transwell experiments were conducted to model the initial uptake of macromolecules and fluid from the interstitium by capillaries. The effective permeability data from both the 3 kDa and 2,000 kDa dextrans showed a slight increase in WT cells over FLOX cells, but this increase is not statistically significant (Figure 11A-B). Also, a relative permeability analysis was

graphed to normalize the 2,000 kDa dextran to the 3 kDa dextran to control for passive barrier integrity (Figure 11C). It does show that the relative permeability of FLOX is higher than WT, but this is statistically insignificant (Figure 11C). Also, the relative permeability data shows that the 2,000 kDa dextran had an 8 to 10-fold concentration difference than 3 kDa (Figure 11C). However, it does not seem congruent that a 2,000 kDa dextran will travel through cells more quickly and efficiently than a 3 kDa dextran. This is most likely due to the fact that the 3 kDa dextran we use is attached to 0.75 dye particles per molecule of dextran while the 2,000 kDa dextran has, on average, 75 dye particle attached to each molecule of dextran. So, the fluorescence may not be giving us the most accurate concentration measurements. Future experiments will correct for this finding. Lastly, our culture conditions and times likely did not produce enough cells for a reliable monolayer, essentially lending these results to be a proof of concept study. This is how future experiments in this project will be analyzed with full confluent monolayers.

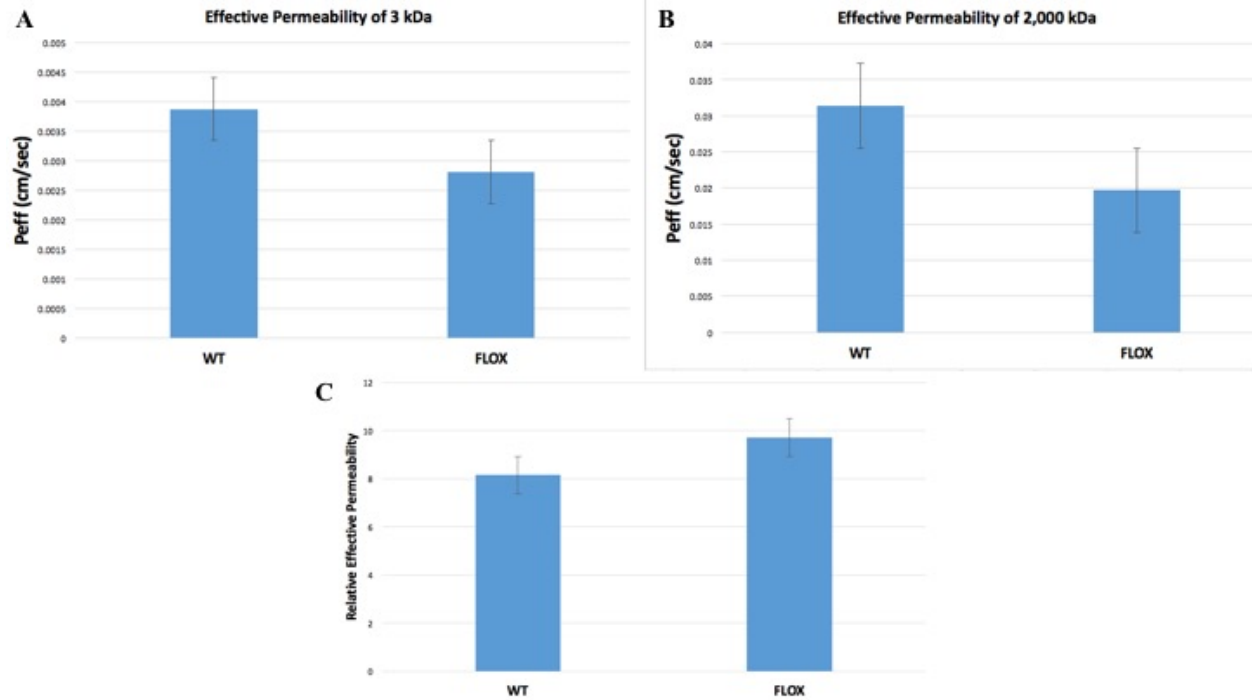


Figure 11. Effective Permeability Results. A) Effective Permeability of 3 kDa dextrans in WT and FLOX cultured cells measured by effective permeability (P_{eff}) seen in Equation 2 with units cm/sec. B) Effective Permeability of 2,000 kDa dextran in WT and FLOX cultured cells measured by effective permeability (P_{eff}) seen in Equation 2 with units cm/sec. C) Relative Effective Permeability used to normalize data to 3 kDa to control for passive barrier integrity.

Lymphatic Vessel Isolation and Permeability Study

We were successfully able to isolate and perfuse a lymphatic vessel running from the inguinal and axillary lymph nodes from the flank of a mouse (Figure 12). A lymphatic vessel section measuring 4 mm in length was successfully isolated and cannulated (Figure 12A). The fluorescent image of the same perfused vessel shows that the fluorescence is defined to the membrane of the lymphatic vessel explaining that the vessel is undamaged and functional (Figure 12B). If the vessel was damaged, fluorescence would be visible outside of the lymphatic vessel membrane in the chamber solution surrounding the vessel.

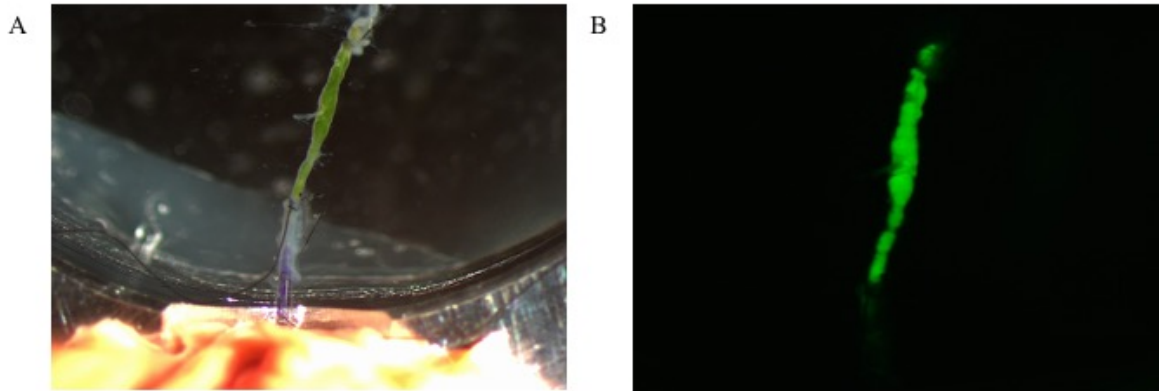


Figure 12. Lymphatic Vessel Isolation. A) A lymphatic vessel (4 mm) is successfully cannulated and pressurized with a fluorescent dextran solution and imaged under white light. B) The same lymphatic vessel from panel A is being imaged using fluorescence.

A permeability study was also conducted to model the transport of macromolecules and fluid in larger lymphatic vessels in between lymph nodes. The kinetic data, while slightly skewed, showed the general trend that we expected (Figure 13). We expected a slow upward trend in both WT and FLOX vessels that was generally observed. However, these results are substantially skewed. But, this is not critical. These experiments were essentially “proof of concept” studies to pave the way for future experiments in the lab with this very detailed and difficult vessel isolation protocol.

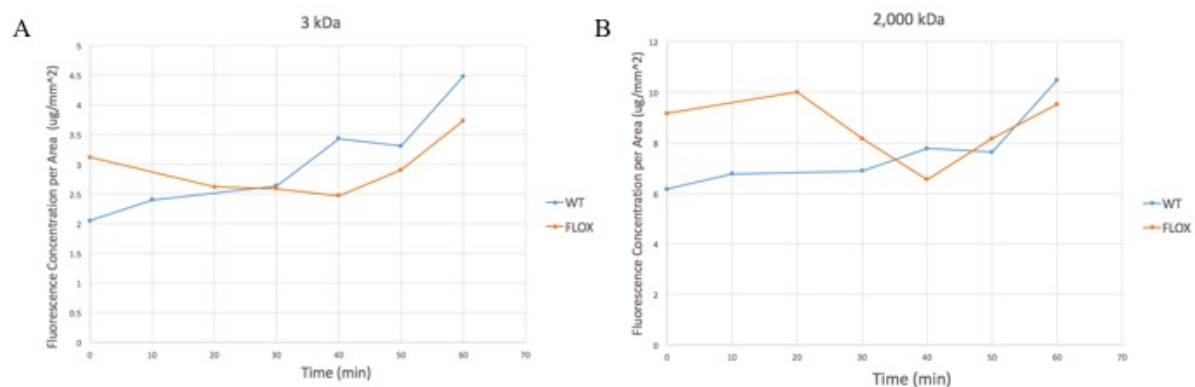


Figure 13. Isolated Vessel Permeability Results. Dextran or Fluorescent concentration per area was measured every 10 minutes for 1 hour.

CHAPTER IV

DISCUSSION

This study focuses on developing protocols for primary LEC isolation and the isolation of intact lymphatic vessels for permeability studies to quantify the role of caveolae in lymphatic macromolecule uptake and transport. These goals were accomplished.

Lymphatic patterning and morphology was an important first experiment because if the architecture of the lymphatic vessels looked vastly different, the subsequent results may be a product of lymphatic structure density (an increase vessel wall surface area ‘S’ from Starling’s equation) and not specifically lymphatic active versus passive transport pathways. The ear lymphatic patterning showed no statistically significant differences in LEC-specific FLOX mice, important for comparing an *in vivo* data. While the KO ears did seem to be slightly hyperplastic this was expected. In KO mice, the entire mouse lacks Cav-1 meaning that the blood vasculature will be much more “leaky” (38, 40) and increased interstitial pressure is expected. Increased IFP forces the lymphatic vessels to slightly expand (42). But, there were no measurable differences in Cav-1 KO tissues meaning that any results from the subsequent experiments could be attributed to the presence or lack of Cav-1 and not the lymphatic architecture.

This led to the first *in vivo* study utilizing footpad injections with differing sized dextrans to measure any transport differences between the three mouse genotypes: WT (Cre-), FLOX (Cre+), and KO. The nomenclature of Cre-/Cre+ indicates whether the Cre recombinase enzyme was ever introduced into the strain. If it was, then Cav-1 was locally deleted in lymphatics, if not, Cav-1 was wild type. Three different sized dextrans were used to test the mouse’s differing abilities to uptake and transport the dextrans through the lymphatics. The sizes were chosen specifically

because of their Stoke's radii. For endothelial layers, solutes with a Stoke's radii of under 3 nm usually travel paracellularly, while molecules with Stoke's radii above 3 nm, like albumin, require transcytosis for appreciable transport (43). In this experiment, the 3 kDa dextran has a Stoke's radius that is much smaller than 3 nm which allows it to easily travel paracellularly while the 70 and 2,000 kDa dextrans have Stoke's radii of 6.4 and 26.89 nm respectively indicating that they require active transport across the membrane (44). So, for WT mice with normal levels of Cav-1, we expect for all the dextrans to be able to be taken up and transported to the axillary because the mice are capable of transcytosis. On the other hand, FLOX mice lack Cav-1 in lymphatics and therefore are incapable of active transport, which we expect would increase paracellular flux and increase dextran transport. An increase in overall lymphatic transport in in cells lacking transcytosis seems paradoxical, but when transcytosis is blocked, this forces the loose overlapping junctions to open much wider than usual allowing large molecules to be taken in. This trend should also be evident in KO mice that have Cav-1 globally deleted because interstitial pressure will increase thus forcing more fluid and macromolecules to be transported transcellularly. The highest concentration of dextrans was found in the skin, while a decaying trend continued to the axillary LN across all three dextran sizes and all three genotypes. These results seem incongruent because if you inject into the footpad, you should expect that the highest level of dextrans will stay in the footpad especially with only 45 minutes given for transport. Also, the axillary LN levels of the dextrans were the lowest because it was the farthest lymph node from the injection site. Although a small hump was observed in the 2,000 kDa popliteal category in FLOXED mice, this was not statistically significant. Overall, there were no remarkable differences in trends between the genotypes and dextran sizes. This could possibly be explained by the fact that the paracellular transport pathway is successfully recovering the transport defects from Cav-1 deleted mice. Most

importantly, the study diverged to focus on the two specific models involved in the *in vivo* injection experiments: initial lymphatic uptake and vessel transport.

To address the role of initial lymphatic uptake of capillaries, we moved our focus from *in vivo* to *in vitro* by specifically isolating and culturing LECs to test the transcellular flux of a LEC monolayer. Following our novel LEC Isolation Protocol rendered cultures that had LEC clusters but with some fibroblast contamination (which outgrow endothelial cells in culture). Although our culture was not a pure LEC population with the hallmark “cobble stone” morphology, we were able to observe interesting growth patterns in the LECs. *In vitro*, LECs are known to grow in a monolayer that when imaged looks like “cobble stones”, while *in vivo* they grow in tube structures forming capillaries and vessels. In our culture, we observed that our LECs grew as if they were *in vivo* forming tube structures on top of a monolayer of fibroblasts (Figure 8). The LEC tubes even were seen to split off into tails stretching out to other LEC clusters (Figure 8D), which is similar to their behavior *in vivo*. Although this growth patterning is rare in tissue culture, it did not render a pure LEC population. To obtain a pure LEC population, a flow sorting experiment was conducted and achieved (Figure 9). Since we are specifically interested in LECs, they are highly LYVE-1 and CD-31 positive since they lymphatics and endothelial cells respectively. This means that P2 in Figure 9 labeled as “LECs” was our pure population that would then be used for transcellular transport studies. However, we needed pure LECs from our three genotypes of interest, WT, FLOX, and KO, to test transcellular flux differences among the three genotypes. To accomplish this, another isolation and flow sort was done to isolate pure LECs from all three genotypes (Figure 10) that were then used in transwell transport experiments.

The transwell transport experiments focused on the change in flux between the monolayer of LECs. Similar to the *in vitro* dextran injection experiments, the chosen dextrans were 3 kDa and

2,000 kDa because the 3 kDa dextran should flow directly through the monolayer paracellularly like normal media due to its small Stoke's radii, while the bulky 2,000 kDa dextran would require active transport to pass the monolayer barrier. The data was focused on a “proof of concept” study because there was insufficient time to grow a reliable monolayer. While the results indicate slight differences in the effective and relative permeabilities, they were not statistically significant (Figure 11). Future experiments will focus on utilizing transendothelial resistance data to ensure a reliable monolayer is present.

Lastly, to test lymphatic vessel permeability *in vivo* more extensively than footpad injections, we developed a Lymphatic Vessel Isolation experimental protocol. This allowed us to take a living lymphatic vessel and test its permeability with differing dextran solutions. We were able to successfully isolate and perfuse an intact lymphatic vessel from the mouse flank and run permeability experiments (Figure 12&13). Since there was no dextran leakage in the fluorescent image, the lymphatic membrane was still intact allowing the vessel to behave as if it were still within the body (Figure 12B). This technique is extremely difficult and specialized – only a handful of groups worldwide successfully employ this method. The vessel isolation technique also opens up a new avenue to study lymphatic vessels *in vivo*. While the initial permeability study showed no novel observations, the procedure and analysis allows us to assess permeability in a novel way that will continue to be utilized in our lab.

To test whether Cav-1 is a critical protein for transcellular transport, two protocols had to be developed: 1) Primary LEC Isolation and 2) Lymphatic Vessel Isolation. These protocols would provide an *in vitro* and an *in vivo* model for Cav-1 respectively and were extremely important for the success of the project. Both of the protocols were successfully developed and tested which allowed for this project to be studied in detail. While the Primary LEC Isolation protocol that we

developed may be a more widespread technique used in mouse lymphatic labs across the country, the success of our Lymphatic Vessel Isolation protocol put us in a category with only a select few labs worldwide that have accomplished this difficult task of isolating a live lymphatic vessel from a mouse. This accomplishment not only benefits this particular project, but it allows for our lab to use a rare novel technique that will bring consistent success.

For future directions, we will focus on perfecting our transwell and permeability experiments. To do this, we must determine whether we have a consistent and reliable monolayer in our transwell plates. This will be accomplished by longer growth times as well as utilizing transendothelial resistance to quantify the growth of our monolayers. We will also continue to perfect our isolation vessel protocol to test if, in fact, mice lacking Cav-1 are more “leaky” than those that are WT. This could explain the results from our *in vivo* study (Figure 7). It is possible that in FLOX mice the initial lymphatics, there is an increase in uptake of macromolecules and fluid, while the larger vessels become “leaky” having a balancing out effect.

Within the field of lymphatics, our data subtly supports the work of Triacca et. al. (2017). However, this project could have implications in not only uptake and transport but also in pumping due to the connections of Cav-1 to the signaling molecule NO involved in lymphatic vasculature permeability and pumping (45-48). Endothelial Nitric-Oxide Synthase (eNOS) specifically targets caveolin-1 which directly inhibits NO production by eNOS (48). This is relevant because eNOS is in charge of making the signaling molecule NO that is responsible for controlling vasomediators and vascular permeability (49-52). Nitric oxide (NO) could be controlling vascular permeability by changing cell morphology and cell junction structures, but the exact mechanism is unknown (45, 46). Overall, Caveolin-1 could be regulating cell permeability not only directly through

transcytosis but also indirectly by prohibiting the production of NO which in turn regulates vasculature permeability (47).

In conclusion, this study focused on the role of Caveolin-1 in transcellular transport of macromolecules. Our results corroborate the results of Triacca et. al. (2017) showing that transcellular transport is in fact important for lymphatic endothelial transport. We also suggest that this is specifically due to the presence of Cav-1 in the caveolae responsible for transcytosis which will be further studied with our pure LEC population and isolated vessels. Overall, the study was successful in developing two protocols that are vital for future research over the role of Cav-1 in macromolecule transport.

REFERENCES

1. Liao S, Padera TP. Lymphatic function and immune regulation in health and disease. *Lymphatic research and biology*. 2013;11(3):136-43.
2. Swartz MA. The physiology of the lymphatic system. *Advanced drug delivery reviews*. 2001;50(1-2):3-20.
3. Traves KP, Studdiford JS, Pickle S, Tully AS. Edema: diagnosis and management. *Am Fam Physician*. 2013;88(2):102-10.
4. Card CM, Yu SS, Swartz MA. Emerging roles of lymphatic endothelium in regulating adaptive immunity. *The Journal of clinical investigation*. 2014;124(3):943-52.
5. Schmid-Schonbein GW. Microlymphatics and lymph flow. *Physiol Rev*. 1990;70(4):987-1028.
6. Leak LV. Studies on the permeability of lymphatic capillaries. *J Cell Biol*. 1971;50(2):300-23.
7. Leak LV. The structure of lymphatic capillaries in lymph formation. *Fed Proc*. 1976;35(8):1863-71.
8. O'Morchoe CC, O'Morchoe PJ. Differences in lymphatic and blood capillary permeability: ultrastructural-functional correlations. *Lymphology*. 1987;20(4):205-9.
9. Sauter B, Foedinger D, Sterniczky B, Wolff K, Rappersberger K. Immunoelectron microscopic characterization of human dermal lymphatic microvascular endothelial cells. Differential expression of CD31, CD34, and type IV collagen with lymphatic endothelial cells vs blood capillary endothelial cells in normal human skin, lymphangioma, and hemangioma in situ. *J Histochem Cytochem*. 1998;46(2):165-76.
10. Baluk P, Fuxe J, Hashizume H, Romano T, Lashnits E, Butz S, et al. Functionally specialized junctions between endothelial cells of lymphatic vessels. *J Exp Med*. 2007;204(10):2349-62.
11. Majno G, Palade GE. Studies on inflammation. 1. The effect of histamine and serotonin on vascular permeability: an electron microscopic study. *J Biophys Biochem Cytol*. 1961;11:571-605.

12. Gerli R, Ibba L, Fruschelli C. A fibrillar elastic apparatus around human lymph capillaries. *Anat Embryol (Berl)*. 1990;181(3):281-6.
13. Ikomi F, Schmid-Schonbein GW. Lymph pump mechanics in the rabbit hind leg. *Am J Physiol*. 1996;271(1 Pt 2):H173-83.
14. Leak LV, Burke JF. Fine structure of the lymphatic capillary and the adjoining connective tissue area. *Am J Anat*. 1966;118(3):785-809.
15. Leak LV, Burke JF. Ultrastructural studies on the lymphatic anchoring filaments. *J Cell Biol*. 1968;36(1):129-49.
16. Schmid-Schonbein GW. Mechanisms causing initial lymphatics to expand and compress to promote lymph flow. *Arch Histol Cytol*. 1990;53 Suppl:107-14.
17. Predescu D, Palade GE. Plasmalemmal vesicles represent the large pore system of continuous microvascular endothelium. *Am J Physiol*. 1993;265(2 Pt 2):H725-33.
18. Predescu D, Vogel SM, Malik AB. Functional and morphological studies of protein transcytosis in continuous endothelia. *Am J Physiol Lung Cell Mol Physiol*. 2004;287(5):L895-901.
19. Rizzo V, Morton C, DePaola N, Schnitzer JE, Davies PF. Recruitment of endothelial caveolae into mechanotransduction pathways by flow conditioning in vitro. *Am J Physiol Heart Circ Physiol*. 2003;285(4):H1720-9.
20. Michel CC, Curry FE. Microvascular permeability. *Physiol Rev*. 1999;79(3):703-61.
21. Samuel SP, Jain N, O'Dowd F, Paul T, Kashanin D, Gerard VA, et al. Multifactorial determinants that govern nanoparticle uptake by human endothelial cells under flow. *Int J Nanomedicine*. 2012;7:2943-56.
22. Schnitzer JE, Oh P, Pinney E, Allard J. Filipin-sensitive caveolae-mediated transport in endothelium: reduced transcytosis, scavenger endocytosis, and capillary permeability of select macromolecules. *J Cell Biol*. 1994;127(5):1217-32.
23. Wagner RC, Chen SC. Transcapillary transport of solute by the endothelial vesicular system: evidence from thin serial section analysis. *Microvasc Res*. 1991;42(2):139-50.
24. Triacca V, Guc E, Kilarski WW, Pisano M, Swartz MA. Transcellular Pathways in Lymphatic Endothelial Cells Regulate Changes in Solute Transport by Fluid Stress. *Circ Res*. 2017.

25. Cheng JP, Nichols BJ. Caveolae: One Function or Many? *Trends Cell Biol.* 2016;26(3):177-89.
26. Farquhar MG, Palade GE. Junctional complexes in various epithelia. *J Cell Biol.* 1963;17:375-412.
27. Yamada E. The fine structure of the gall bladder epithelium of the mouse. *J Biophys Biochem Cytol.* 1955;1(5):445-58.
28. Feng D, Nagy JA, Dvorak HF, Dvorak AM. Ultrastructural studies define soluble macromolecular, particulate, and cellular transendothelial cell pathways in venules, lymphatic vessels, and tumor-associated microvessels in man and animals. *Microsc Res Tech.* 2002;57(5):289-326.
29. Dixon JB, Raghunathan S, Swartz MA. A tissue-engineered model of the intestinal lacteal for evaluating lipid transport by lymphatics. *Biotechnol Bioeng.* 2009;103(6):1224-35.
30. Lim HY, Thiam CH, Yeo KP, Bisoendial R, Hii CS, McGrath KC, et al. Lymphatic vessels are essential for the removal of cholesterol from peripheral tissues by SR-BI-mediated transport of HDL. *Cell Metab.* 2013;17(5):671-84.
31. Reed AL, Rowson SA, Dixon JB. Demonstration of ATP-dependent, transcellular transport of lipid across the lymphatic endothelium using an in vitro model of the lacteal. *Pharm Res.* 2013;30(12):3271-80.
32. Drab M, Verkade P, Elger M, Kasper M, Lohn M, Lauterbach B, et al. Loss of caveolae, vascular dysfunction, and pulmonary defects in caveolin-1 gene-disrupted mice. *Science.* 2001;293(5539):2449-52.
33. Fra AM, Williamson E, Simons K, Parton RG. De novo formation of caveolae in lymphocytes by expression of VIP21-caveolin. *Proc Natl Acad Sci U S A.* 1995;92(19):8655-9.
34. Glenney JR, Jr. Tyrosine phosphorylation of a 22-kDa protein is correlated with transformation by Rous sarcoma virus. *J Biol Chem.* 1989;264(34):20163-6.
35. Glenney JR, Jr. The sequence of human caveolin reveals identity with VIP21, a component of transport vesicles. *FEBS Lett.* 1992;314(1):45-8.
36. Li S, Song KS, Koh SS, Kikuchi A, Lisanti MP. Baculovirus-based expression of mammalian caveolin in Sf21 insect cells. A model system for the biochemical and morphological study of caveolae biogenesis. *J Biol Chem.* 1996;271(45):28647-54.

37. Murata M, Peranen J, Schreiner R, Wieland F, Kurzchalia TV, Simons K. VIP21/caveolin is a cholesterol-binding protein. *Proc Natl Acad Sci U S A*. 1995;92(22):10339-43.
38. Razani B, Engelman JA, Wang XB, Schubert W, Zhang XL, Marks CB, et al. Caveolin-1 null mice are viable but show evidence of hyperproliferative and vascular abnormalities. *J Biol Chem*. 2001;276(41):38121-38.
39. Scherer PE, Lewis RY, Volonte D, Engelman JA, Galbiati F, Couet J, et al. Cell-type and tissue-specific expression of caveolin-2. Caveolins 1 and 2 co-localize and form a stable hetero-oligomeric complex in vivo. *J Biol Chem*. 1997;272(46):29337-46.
40. Schubert W, Frank PG, Razani B, Park DS, Chow CW, Lisanti MP. Caveolae-deficient endothelial cells show defects in the uptake and transport of albumin in vivo. *J Biol Chem*. 2001;276(52):48619-22.
41. Rutkowski JM, Pastor J, Sun K, Park SK, Bobulescu IA, Chen CT, et al. Adiponectin alters renal calcium and phosphate excretion through regulation of klotho expression. *Kidney Int*. 2017;91(2):324-37.
42. Wiig H, Swartz MA. Interstitial fluid and lymph formation and transport: physiological regulation and roles in inflammation and cancer. *Physiol Rev*. 2012;92(3):1005-60.
43. Mehta D, Malik AB. Signaling mechanisms regulating endothelial permeability. *Physiol Rev*. 2006;86(1):279-367.
44. Armstrong JK, Wenby RB, Meiselman HJ, Fisher TC. The hydrodynamic radii of macromolecules and their effect on red blood cell aggregation. *Biophys J*. 2004;87(6):4259-70.
45. Garcia JG, Schaphorst KL. Regulation of endothelial cell gap formation and paracellular permeability. *J Investig Med*. 1995;43(2):117-26.
46. Lum H, Malik AB. Regulation of vascular endothelial barrier function. *Am J Physiol*. 1994;267(3 Pt 1):L223-41.
47. Schubert W, Frank PG, Woodman SE, Hyogo H, Cohen DE, Chow CW, et al. Microvascular hyperpermeability in caveolin-1 (-/-) knock-out mice. Treatment with a specific nitric-oxide synthase inhibitor, L-NAME, restores normal microvascular permeability in Cav-1 null mice. *J Biol Chem*. 2002;277(42):40091-8.

48. Bucci M, Gratton JP, Rudic RD, Acevedo L, Roviezzo F, Cirino G, et al. In vivo delivery of the caveolin-1 scaffolding domain inhibits nitric oxide synthesis and reduces inflammation. *Nat Med.* 2000;6(12):1362-7.
49. Hood JD, Meininger CJ, Ziche M, Granger HJ. VEGF upregulates ecNOS message, protein, and NO production in human endothelial cells. *Am J Physiol.* 1998;274(3 Pt 2):H1054-8.
50. Lal BK, Varma S, Pappas PJ, Hobson RW, 2nd, Duran WN. VEGF increases permeability of the endothelial cell monolayer by activation of PKB/akt, endothelial nitric-oxide synthase, and MAP kinase pathways. *Microvasc Res.* 2001;62(3):252-62.
51. Ramirez MM, Quardt SM, Kim D, Oshiro H, Minnicozzi M, Duran WN. Platelet activating factor modulates microvascular permeability through nitric oxide synthesis. *Microvasc Res.* 1995;50(2):223-34.
52. Yuan Y, Granger HJ, Zawieja DC, DeFily DV, Chilian WM. Histamine increases venular permeability via a phospholipase C-NO synthase-guanylate cyclase cascade. *Am J Physiol.* 1993;264(5 Pt 2):H1734-9.

APPENDIX

Lymphangiogenesis: fuel, smoke, or extinguisher of inflammation's fire?

Gabriella R Abouelkheir, Bradley D Upchurch and Joseph M Rutkowski

Division of Lymphatic Biology, Department of Medical Physiology, Texas A&M College of Medicine, College Station, TX 77843, USA Corresponding author: Joseph M Rutkowski. Email: rutkowski@tamu.edu

Impact statement

Inflammatory progression is present in acute and chronic tissue pathologies throughout the body. Lymphatic vessels play physiological roles relevant to all medical fields as important regulators of fluid balance, immune cell trafficking, and immune identity. Lymphangiogenesis is often concurrent with inflammation and can potentially aide or worsen disease progression. How new lymphatic vessels impact inflammation and by which mechanism is an important consideration in current and future clinical therapies targeting inflammation and/or vasculogenesis. This review identifies, across a range of tissue-specific pathologies, the current understanding of inflammation-associated lymphangiogenesis in the progression or resolution of inflammation.

Abstract

Lymphangiogenesis is a recognized hallmark of inflammatory processes in tissues and organs as diverse as the skin, heart, bowel, and airways. In clinical and animal models wherein the signaling processes of lymphangiogenesis are manipulated, most studies demonstrate that an expanded lymphatic vasculature is necessary for the resolution of inflammation. The fundamental roles that lymphatics play in fluid clearance and immune cell trafficking from the periphery make these results seemingly obvious as a mechanism of alleviating locally inflamed environments: the lymphatics are simply providing a drain. Depending on the tissue site, lymphangiogenic mechanism, or induction timeframe, however, evidence shows that inflammation-associated lymphangiogenesis (IAL) may worsen the pathology. Recent studies have identified lymphatic endothelial cells themselves to be local regulators of immune cell activity and its consequential phenotypes – a more active role in inflammation regulation than previously thought. Indeed, results focusing on the immunocentric roles of peripheral lymphatic function have revealed that the basic drainage task of lymphatic vessels is a complex balance of locally processed and transported antigens as well as interstitial cytokine and immune cell signaling: an interplay that likely defines the function of IAL. This review will summarize the latest findings on how IAL impacts a series of disease states in various tissues in both preclinical models and clinical studies. This discussion will serve to highlight some emerging areas of lymphatic research in an attempt to answer the question relevant to an array of scientists and clinicians of whether IAL helps to fuel or extinguish inflammation.

Keywords: Vascular endothelial growth factor receptor-3, lymphatic, vascular endothelial growth factor-D, metabolic syndrome, endometriosis, hypertension

Experimental Biology and Medicine 2017; 242: 884–895. DOI: 10.1177/1535370217697385

This document is accessible by searching this DOI: 10.1177/1535370217697385